ARTICLE　　　　　　　　　　　　　　　　　　　　　　　**Open Access**

Narrow band-edge photoluminescence from AgInS$_2$ semiconductor nanoparticles by the formation of amorphous III–VI semiconductor shells

Taro Uematsu[1,2], Kazutaka Wajima[2], Dharmendar Kumar Sharma[3], Shuzo Hirata[3], Takahisa Yamamoto[4], Tatsuya Kameyama[5], Martin Vacha[3], Tsukasa Torimoto [5] and Susumu Kuwabata[2]

Abstract
Nanoparticles of I–III–VI semiconductors are promising candidates for novel non-toxic fluorescent materials. However, removal of defect levels responsible for their broad-band emission has not been successful to date. The present study demonstrates, for the first time, the coating of core AgInS$_2$ nanoparticles—one of the I–III–VI group semiconductors with a bandgap in the visible region—with III–VI group semiconductors. The AgInS$_2$/InS$_x$ and AgInS$_2$/GaS$_x$ ($x = 0.8$–1.5) core/shell structures generate intense narrow-band photoluminescence originating from a band-edge transition at a wavelength shorter than that of the original defect emission. Microscopic analyses reveal that the GaS$_x$ shell has an amorphous nature, which is unexpected for typical shell materials such as crystalline lattice-matching ZnS. Single-particle spectroscopy shows that the average linewidth of the band-edge photoluminescence is as small as 80.0 meV (or 24 nm), which is comparable with that of industry-standard II–VI semiconductor quantum dots. In terms of photoluminescence quantum yield, a value of 56% with nearly single-band emission has been achieved as a result of several modifications to the reaction conditions and post-treatment to the core/shell nanoparticles. This work indicates the increasing potential of AgInS$_2$ nanoparticles for use as practical cadmium-free quantum dots.

Introduction

Semiconductor nanoparticles of sufficiently small size have their optical properties determined by quantum confinement, which causes a shift in the energy of an optical transition with crystal size. Such semiconductor nanoparticles (NPs), or quantum dots (QDs), have attracted considerable attention following the development of methods for synthesizing highly monodisperse, well-stabilized, and intensely emitting NPs[1,2]. Cadmium

selenide and its alloys with other II–VI semiconductors have been at the center of research activities due to their narrow band-edge emission deriving from their characteristics as direct semiconductors[3]. In addition to being the subject of academic and industrial research, CdSe and other II–VI semiconductor QDs have been increasingly finding commercial applications in liquid-crystal displays and television sets to optimize the color composition of backlights, in lighting to improve the quality of light for specific applications and in biological research as labels for bioimaging and drug-delivery components[4]. With the rapid spread of applications, however, the high toxicity of cadmium is becoming a matter of increasing concern, and CdSe and related QD materials are likely to face a ban in many countries. The search for a replacement for toxic CdSe QDs with non-toxic alternatives with comparable

Correspondence: Martin Vacha (vacha.m.aa@m.titech.ac.jp) or
Tsukasa Torimoto (torimoto@chembio.nagoya-u.ac.jp) or Susumu Kuwabata
(kuwabata@chem.eng.osaka-u.ac.jp)
[1]Frontier Research Base for Global Young Researchers, Graduate School of
Engineering, Osaka University, 2-1 Yamada-oka, Suita, Osaka 565-0871, Japan
[2]Department of Applied Chemistry, Graduate School of Engineering, Osaka
University, 2-1 Yamada-oka, Suita, Osaka 565-0871, Japan
Full list of author information is available at the end of the article.

properties, such as stability, size monodispersity, high emission quantum yield (QY), narrow-band emission spectrum and chemical 'wet' preparation, is therefore an utmost priority for many research groups. Recent attempts to substitute other materials for toxic cadmium have successfully utilized III–V semiconductors such as InP, InAs, and GaAs[5–7] and I–III–VI ternary semiconductors represented by CuInS$_2$, AgInS$_2$, and their selenide derivatives[8–11]. Although the quantum yield of the latter has been improved to exceed 50%, the lack of monochromaticity of their photoluminescence (PL), represented by broad PL spectra, has been recognized as a major problem[12–14]. There are at least two possible origins of the spectrally broad PL from ternary semiconductor QDs: defects on the particle surface and/or defects inside the crystals. The structural diversity characteristic of ternary materials is considered to be the origin of various donor–acceptor levels, which have recently been identified by PL decay and single-particle analyses[15]. Efforts to generate intense, defect-free semiconductor band-edge PL from I–III–VI semiconductor nanomaterials have not been successful to date. Some researchers have even concluded from time-resolved and X-ray measurements that emission originating from several sets of donor–acceptor pairs is inevitably generated in I–III–VI-based and I–III–VI-based semiconductor nanomaterials, giving rise to PL spectra with a full width at half maximum (FWHM) larger than 100 nm, or 300 meV[13,14,16]. Although recent studies by our group on AgInTe$_2$ nanorods have led to a relatively narrow emission (FWHM of 100–150 nm or 110–180 meV) in the infrared region (with PL peak of 1000–1100 nm), the PL origin was attributed to donor–acceptor transitions located close to the band edge[17].

In the present study, we developed a reproducible method for obtaining spectrally narrow band-edge PL from AgInS$_2$ NPs in the visible region. The band-edge emission was achieved by coating AgInS$_2$ NP cores, synthesized by a conventional heating method, with III–VI group semiconductor shells. As a result, we observed PL that was nearly an order of magnitude narrower than that of uncoated AgInS$_2$ NPs (FWHM of 28.6 nm, or 103 meV, compared with FWHM of 220 nm, or 388 meV, respectively). Single-particle analysis revealed even higher monochromaticity at the single-NP level, with an average PL spectral width FWHM of 24.0 nm (or 80.0 meV) at room temperature. This value is now fully comparable with that of industry-standard II–VI semiconductor QDs, such as CdSe and CdTe[3], and less than half of that of other alternative cadmium-free QDs, such as InP[7]. The final section discusses the great potential of these cadmium-free QDs by demonstrating a several-fold improvement of PL QY as a result of modifications to the synthetic conditions and post-treatment of the as-synthesized core/shell NPs. At present, QDs with a PL QY as high as 56% have been obtained reproducibly.

Materials and methods
Chemicals

Silver acetate (Ag(OAc), Wako), In(OAc)$_3$ (Aldrich), Ga (acac)$_3$ (Aldrich), 1-dodecanethiol (Wako), tri-*n*-octylphosphine (TOP, TCI), thiourea (Kishida Chemical Co., Ltd), 1,3-dimethylthiourea (TCI), and elemental sulfur (5N, Mitsuwa Chemical Co., Ltd) were used without further purification. Oleylamine (Aldrich) was used after vacuum distillation in the presence of calcium hydride.

Instrumental

In the synthesis procedures, samples were heated in a two-neck flask using a heating mantle. The solution temperature was directly measured, and the heater was controlled to fix the solution temperature. PL and UV–vis spectra were recorded with a multichannel PL analyzer (Hamamatsu, PMA-12) and a UV–vis spectrometer (JASCO, V-670). PL QYs were measured by attaching an integrating sphere to the PL spectrometer. PL lifetimes were recorded with a time-correlated single-photon counting setup (Hamamatsu, Quantaurus-Tau). Electron microscopy observations were performed with a Hitachi H-7650 TEM (an acceleration voltage: 100 kV) for TEM and Cs-corrected HR-STEM (JEM-ARM-200F, JEOL Co. Ltd., an acceleration voltage: 200 kV) for high-resolution TEM (HRTEM) and high-angle annular dark-field scanning transmission electron microscopy (HAADF-STEM). XRD patterns were recorded with a powder X-ray analysis apparatus (Rigaku, SmartLab) equipped with a parallel-beam/parallel-slit analyzer. XPS spectra were recorded with an X-ray photoelectron spectrometer (Shimadzu, KRATOS AXIS-165x) equipped with an aluminum target. The apparatuses used for single-particle measurements are described in a separate section below.

Synthesis of AgInS$_2$ NPs at constant heating rate

In a two-neck flask, Ag(OAc) (0.4 mmol) and In(OAc)$_3$ (0.4 mmol) were mixed with thiourea (0.8 mmol) in 12 mL of an oleylamine/1-dodecanethiol mixed solvent, typically in a ratio of 59/1 (vol/vol). The mixture was degassed and filled with Ar, heated to 200 °C at a rate of 10 °C/min and then cooled to room temperature. After removing large precipitates by centrifugation, a clear red solution was obtained. The smallest possible amount of methanol was added to precipitate the NPs. After centrifugation, AgInS$_2$ NPs capped with oleylamine were obtained as a solid.

Synthesis of III–VI semiconductor shells from elemental sulfur

Oleylamine-capped AgInS$_2$ NPs (30 nmol in terms of particle) were dissolved in 12 mL oleylamine, and then

either In(OAc)$_3$ or Ga(acac)$_3$ (0.1 mmol) and elemental sulfur (0.15 mmol) were mixed at room temperature. The mixture was degassed and filled with argon, then heated to 200 °C (InS$_x$ shell) or 260 °C (GaS$_x$ shell) at a rate of 10 °C/min. The temperature was held constant for 60 min, and aliquots of the mixture were removed from the flask intermittently for PL measurements. The resulting AgInS$_2$/GaS$_x$ core/shell NPs were purified by precipitating with methanol followed by centrifugation, and the solid was dissolved in hexane.

Synthesis of small AgInS$_2$ NPs at low temperature

For AgInS$_2$ core NPs, a slight modification to the aforementioned method improved the monodispersity. Ag(OAc) (0.4 mmol) and In(OAc)$_3$ (0.4 mmol) were mixed with oleylamine (8 mL) and 1-dodecanethiol (1.25 mmol), and the temperature was then increased to approximately 80 °C under an Ar atmosphere. Thiourea, recrystallized from water, was added to the flask, and the temperature was increased to 135 °C at a rate of 30 °C/min with stirring. The temperature was maintained for 10 min and then cooled to room temperature immediately by dipping the flask into a water bath (25 °C). The NPs were purified as described in the previous section and dispersed in oleylamine (2 mL).

Synthesis of GaS$_x$ semiconductor shells from 1,3-dimethylthiourea

Approximately 30 nmol (in terms of NPs) of AgInS$_2$ core NPs were mixed with an oleylamine (7 mL) suspension containing Ga(acac)$_3$ (0.1 mmol) and 1,3-dimethylthiourea (0.1 mmol). The reaction mixture was heated rapidly to 230 °C, and the temperature was then increased to 280 °C at 2 °C/min under an Ar atmosphere. The solution was then cooled to room temperature in air, during which the solution was degassed for several minutes to remove volatile, unreacted sulfur species. The core/shell NPs were purified as previously described and then dissolved in chloroform (4 mL). Finally, the same volume of TOP was added to the chloroform solution and incubated for several hours at room temperature.

Single-particle measurements

Single-particle imaging and spectroscopy were performed on an epifluorescence microscope setup. Briefly, an inverted optical microscope (Olympus, IX71) equipped with a high-numerical-aperture objective (Olympus, UPlan FLN 100×/1.3 NA, Oil) was used for PL imaging. Samples were excited with a 375 nm (~13 W cm^{-2}) diode laser (PicoQuant, LDH-PC-375), and PL was detected using electron-multiplying CCD camera (Andor Technology, iXon) after passing through an imaging spectrograph (Bunkou Keiki, CLP-50, 0.5 nm resolution). A 400 nm longpass filter (Thorlabs, FELH0400) was used to suppress unwanted excitation and scattered light in the detection path. Data were recorded as image sequences at 0.05 s (20 Hz) and 1 s (1 Hz) acquisition times for imaging and spectroscopy, respectively. All single-particle measurements were performed at 295 K under a N$_2$ environment. For sample preparation, AgInS$_2$/Ga$_2$S$_3$ core/shell NPs were dispersed in toluene and spun-cast onto pre-cleaned quartz coverslips (1 × 0.2, Technical Glass Products) at 2000 rpm. The concentration of NPs was optimized to obtain well-separated (typically with 1 μm interval) and randomly distributed diffraction-limited emission spots (Fig. S1a–c, supplementary information). Well-separated spots showing characteristic single-step blinking and photobleaching (Fig. S1d, supplementary information) were considered to have originated from a single emitter.

Results and discussion

Choice of shell materials

Preparation of a type I core/shell structure, meaning that the bandgap of the shell covers the bandgap of the core, is a common strategy for obtaining strong and stable emission from semiconductor NPs[18]. Zinc sulfide (ZnS) has been widely used as a shell material for II–VI and III–V semiconductor NPs because of its chemical stability, high crystallinity, and wide bandgap (3.7 eV), which is crucial for type I band alignment. Coating with ZnS has also been attempted for CuInS$_2$ ternary NPs by reacting them with a mixed solution of zinc and sulfur sources[19]. The treatment resulted in blueshifts in PL, in contrast to the redshift generally observed for semiconductor NPs after overcoating with larger-bandgap semiconductors. The expected redshift is usually explained by the leakage of excitons from the core into the shell, whose bandgap is essentially smaller than the HOMO-LUMO gap of insulating organic ligands on its surface[20]. The blueshift, in contrast, is often explained as the result of changes in surface defect levels by surface passivation with ZnS and/or the result of partial alloying by cation exchange from copper and indium into zinc[21−23]. In our experiments, we also observed a blueshift in PL when AgInS$_2$ NPs were reacted with zinc acetate (Zn(OAc)$_2$) and elemental sulfur at 200 °C, as shown in the optical spectra in Fig. 1a, b.

According to the abovementioned considerations, the semiconductor used for the shell should be selected from materials that do not easily form alloys, or solid solutions, with the core NPs. However, the formation of defect levels between the core and shell must be avoided. Considering the band-edge criteria for the type I core/shell structure, indium sulfide, which shares two of the three elements composing the core AgInS$_2$ and has a wider bandgap (2.2 eV) than that of the core (1.8 eV for bulk), emerged as a candidate material. The phase diagram for the Ag$_2$S–In$_2$S$_3$ quasi-binary system shows that AgInS$_2$ forms continuous
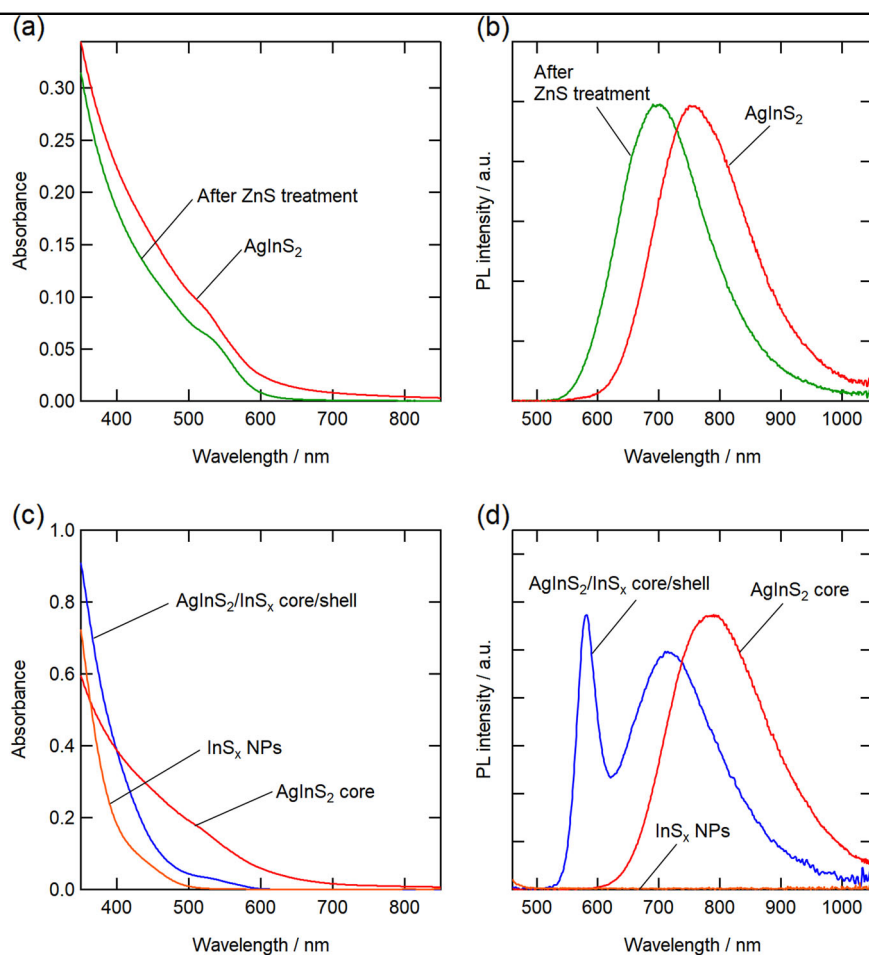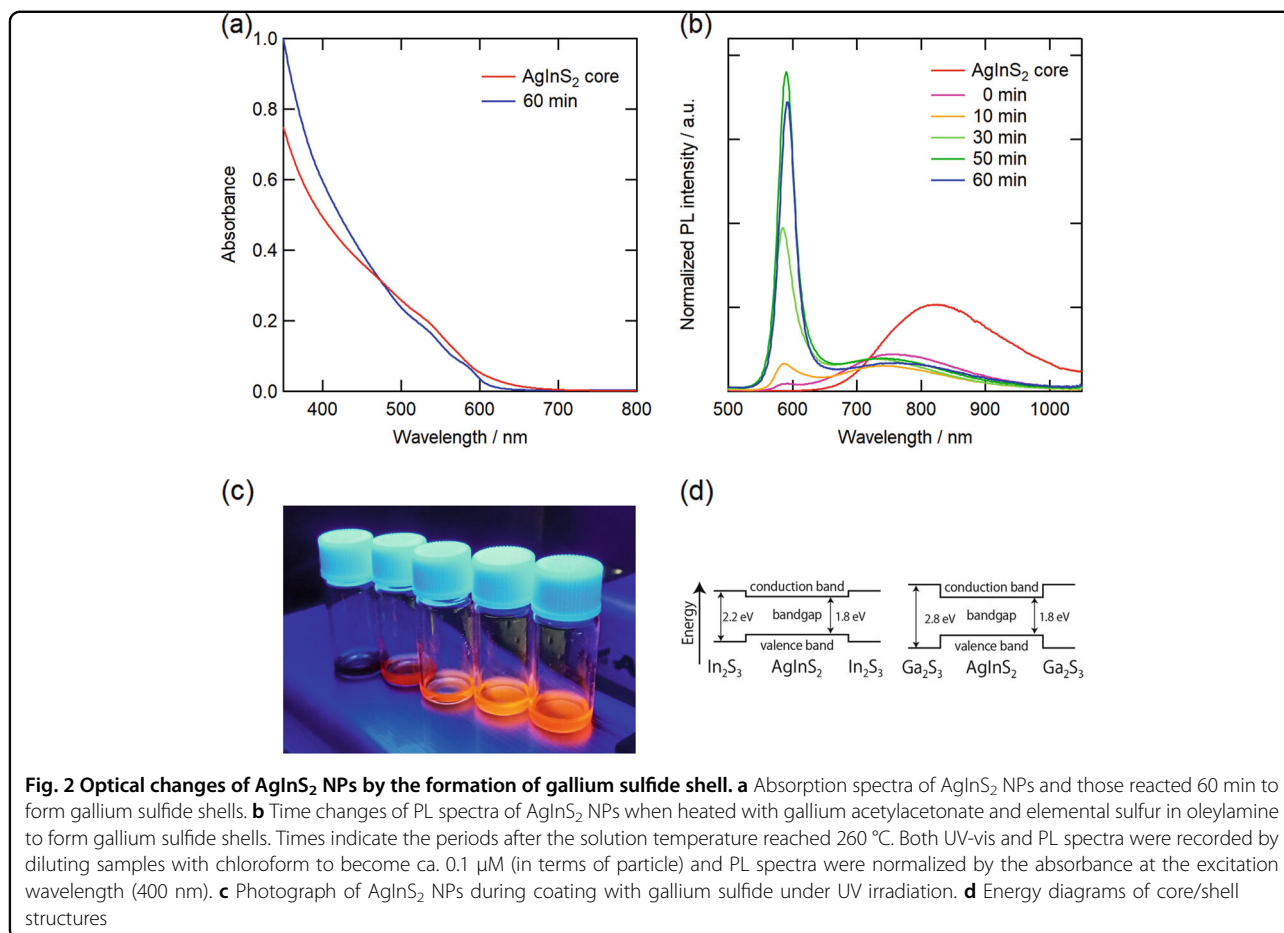
Fig. 1 UV-vis and PL spectra of AgInS$_2$ NPs coated with different semiconductors. a UV-vis and **b** PL spectra of AgInS$_2$ NPs synthesized with the heating up approach and the same NPs after the reaction with zinc acetate and elemental sulfur to form ZnS shells. **c** UV-vis and **d** PL spectra of AgInS$_2$ NPs, InS$_x$ NPs, and AgInS$_2$ NPs after the reaction with indium acetate and elemental sulfur to form indium sulfide shells. The excitation wavelength was 450 nm for all spectra. Samples were diluted with chloroform to become ca. 0.1 μM in terms of particle upon measurements

solid solution series with In$_2$S$_3$ only within a limited region of high indium content (81–96% In$_2$S$_3$)[24], which is less miscible than with ZnS[25]. Figure 1c, d shows UV–vis absorption and PL spectra obtained after the AgInS$_2$ core NPs were reacted with indium acetate (In(OAc)$_3$) and elemental sulfur. The indium sulfide (InS$_x$) shell was synthesized by slowly increasing the temperature of the oleylamine solution of the AgInS$_2$ core in the presence of these precursors (10 °C/min up to 200 °C) and maintaining this temperature for 1 h. The resulting PL spectrum was apparently different from that of the ZnS coating, with the emergence of a new narrow PL peak on the short-wavelength side of the original defect emission. In contrast, InS$_x$ NPs synthesized by a method similar to that used for the shell coating was completely non-luminescent, confirming that the narrow PL peak originated from the AgInS$_2$/InS$_x$ core/shell structure. However, due to insufficient passivation, substantial broad emission persisted, with a blueshift of 70 nm, suggesting that part of

the indium source participated in changing the core composition to an indium-rich form (e.g., AgIn$_5$S$_8$) during the reaction[26].

The monochromaticity of the emission was further greatly improved by coating the AgInS$_2$ core NPs with gallium sulfide (GaS$_x$) instead of with InS$_x$. First, a structure composed of several shoulders appeared in the UV–vis spectrum, resembling the absorption of size-quantized, well-stabilized semiconductor QDs (Fig. 2a)[27]. In Fig. 2b, PL spectra are shown for different elapsed times (0–60 min) after the reaction temperature reached 260 °C. The broad-band defect emission (>600 nm) of the uncoated AgInS$_2$ NPs decreased with the formation of the gallium sulfide shell, followed by the appearance of a new narrow peak on the short-wavelength side of the defect emission, as demonstrated in the imaged obtained under UV illumination (Fig. 2c). Similarly to the indium sulfide of the same group, no single phase has been reported between AgInS$_2$ and Ga$_2$S$_3$ according to the quasi-ternary

Fig. 2 Optical changes of AgInS₂ NPs by the formation of gallium sulfide shell. a Absorption spectra of AgInS$_2$ NPs and those reacted 60 min to form gallium sulfide shells. **b** Time changes of PL spectra of AgInS$_2$ NPs when heated with gallium acetylacetonate and elemental sulfur in oleylamine to form gallium sulfide shells. Times indicate the periods after the solution temperature reached 260 °C. Both UV-vis and PL spectra were recorded by diluting samples with chloroform to become ca. 0.1 μM (in terms of particle) and PL spectra were normalized by the absorbance at the excitation wavelength (400 nm). **c** Photograph of AgInS$_2$ NPs during coating with gallium sulfide under UV irradiation. **d** Energy diagrams of core/shell structures

phase diagram of Ag$_2$S, In$_2$S$_3$, and Ga$_2$S$_3$[28]. The great improvement of monochromaticity might be attributed to the wider bandgap of gallium sulfide (2.8 eV) compared with that of indium sulfide (2.2 eV) (Fig. 2d). The similarity in wavelength of the newly generated PL peaks between InS$_x$ and GaS$_x$-coated AgInS$_2$ NPs ruled out the possibility of cation exchange between indium in the core and gallium in the shell.

To the best of our knowledge, such drastic changes in the PL and UV–vis spectra only appeared when the AgInS$_2$ NPs were reacted with indium (III) or gallium (III) species in the presence of sulfur and were not been observed when the mixture was heated in the absence of one or both precursor materials. When the core NPs were heated at 270 °C for 1 h in oleylamine without adding any precursor materials, the NPs partially agglomerated and the quantum yield decreased by approximately 80%, possibly due to Ostwald ripening (Figure S2, supplementary information). Therefore, the emergence of narrowband emission, which reflects a diminishing contribution of the defect sites to the PL, likely originated from the NPs' surface modification, rather than from the removal of defect levels inside the crystals or the transformation of the crystalline phase by the applied heat.

Several studies have investigated the mechanism of broad defect emission with a large Stokes shift[13,14,16,26]. The defect emission is often explained in relation to the existence of localized donor defect or acceptor defect states caused by vacancies, interstitials or anti-sites within the crystal structure or by structural defects on the surface. The defect states are often proposed to explain the fact that the actual composition of I–III–VI semiconductors often deviates from the stoichiometric composition. However, the present results indicate the prevailing importance of surface conditions in generating band-edge emission.

Origin of narrow-band emission

Figure 3a shows PL spectra of the original bare AgInS$_2$ NPs and of those coated with gallium sulfide in chloroform after isolation of the NPs via the precipitation/dissolution method. The PL QY was 12.4% for the sharp band emission (530–630 nm) and 21.7% for the entire PL range (530–900 nm). The narrowband emission of the core/shell NPs had a FWHM as small as 28.6 nm (103 meV), much smaller than that of the uncoated AgInS$_2$ NPs (220 nm, 388 meV). The corresponding photoluminescence excitation (PLE) spectra recorded at the
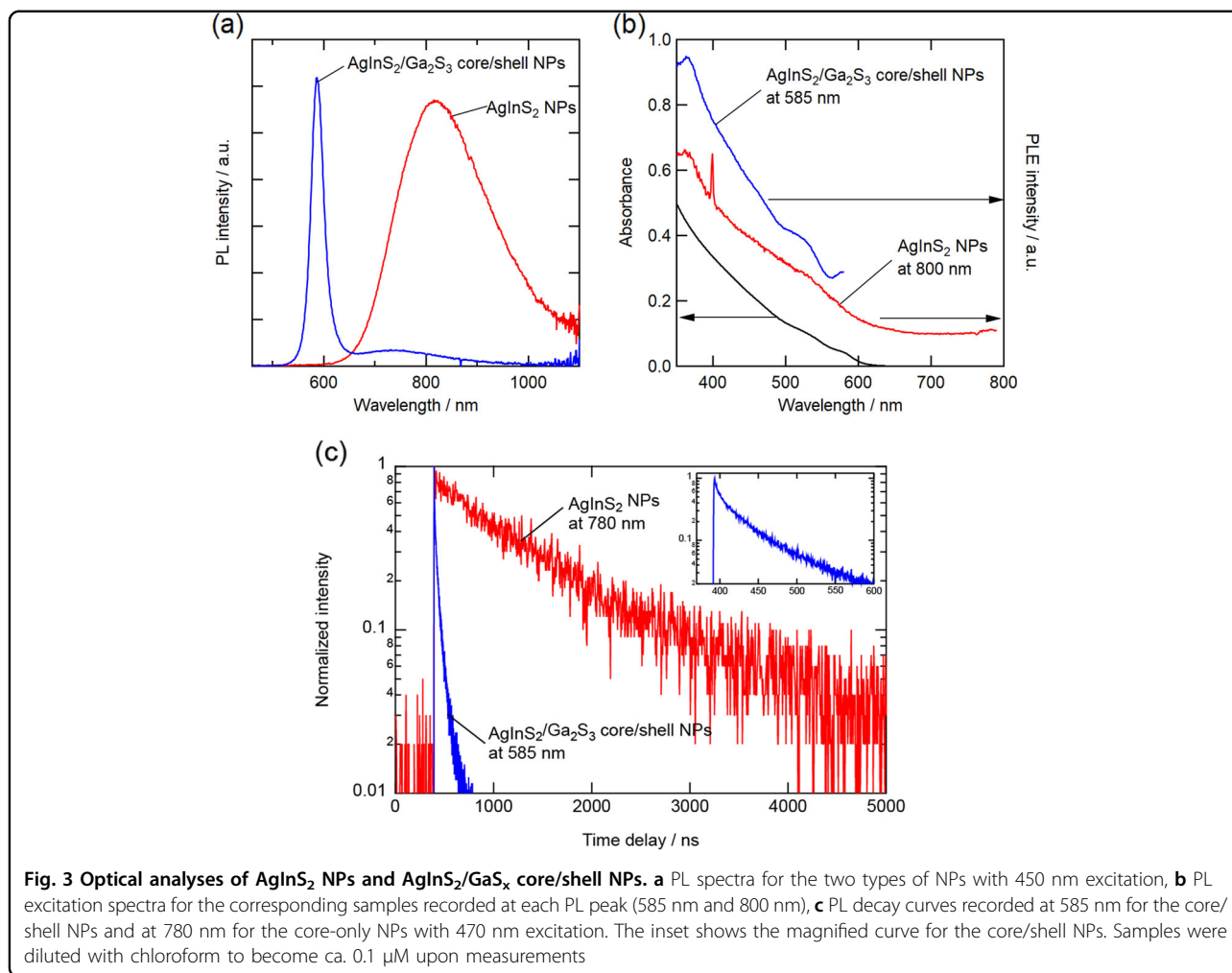
Fig. 3 Optical analyses of AgInS$_2$ NPs and AgInS$_2$/GaS$_x$ core/shell NPs. a PL spectra for the two types of NPs with 450 nm excitation, **b** PL excitation spectra for the corresponding samples recorded at each PL peak (585 nm and 800 nm), **c** PL decay curves recorded at 585 nm for the core/ shell NPs and at 780 nm for the core-only NPs with 470 nm excitation. The inset shows the magnified curve for the core/shell NPs. Samples were diluted with chloroform to become ca. 0.1 μM upon measurements

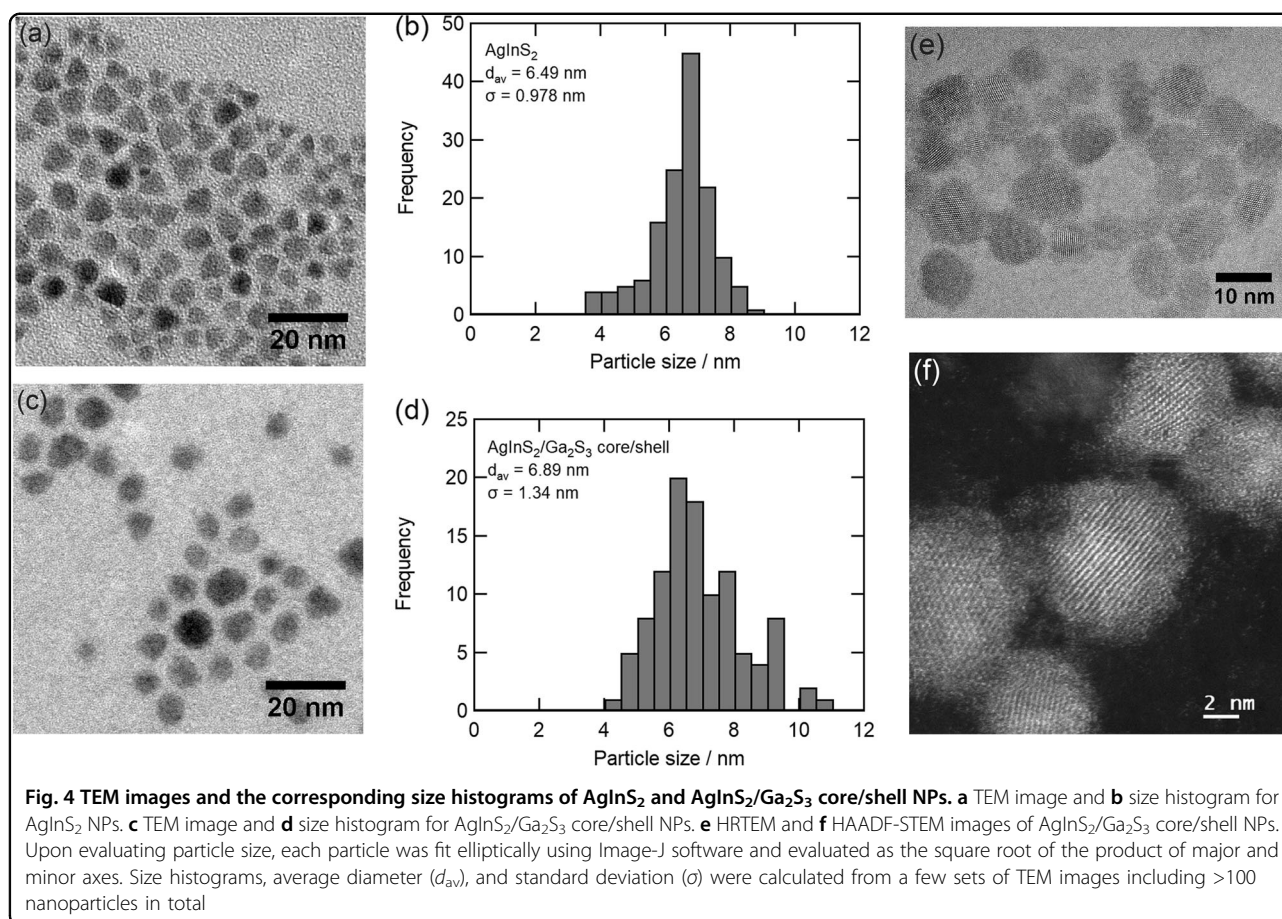**Table 1 PL decay components for AgInS$_2$ NPs and AgInS$_2$/GaS$_x$ core/shell NPs**

Sample		A_1, τ_1	A_2, τ_2	A_3, τ_3	x^2
AgInS$_2$ (780 nm)	A	1	–	–	1.06
	τ/ns	919.0	–	–	
AgInS$_2$/Ga$_2$S$_3$ core/shell (585 nm)	A	0.587	0.320	0.093	1.26
	τ/ns	1.4	24.8	96.6	

respective peak wavelengths are shown in Fig. 3b, along with a UV–vis spectrum of the core/shell NPs. A distinct excitonic feature at 530 nm was observed for the excitation spectrum of the core/shell NPs only, whereas the uncoated AgInS$_2$ NPs showed a monotonic increase in PL intensity with decreasing excitation wavelength. The PL decay curves in Fig. 3c show a significant decrease in the lifetime components for the core/shell NPs compared with those of the uncoated AgInS$_2$ NPs. The decay curves for the core/shell NPs were fitted to a three-exponential

equation:

$$I(t) = A_1 \exp\left(-\frac{t}{\tau_1}\right) + A_2 \exp\left(-\frac{t}{\tau_2}\right) + A_3 \exp\left(-\frac{t}{\tau_3}\right),$$

where $I(t)$ is the PL intensity at time t; A_1, A_2, and A_3 are amplitudes; and τ_1, τ_2, and τ_3 are lifetimes. In contrast, the decay curve of the uncoated AgInS$_2$ NPs was sufficiently fit with a single-component exponential. The fitting results are summarized in Table 1. For the core/shell NPs, the second component (24.8 ns) contributed to 45% of the total emission intensity and the third component (96.6 ns) contributed to 50% of the total emission intensity compared with the components described in terms of products of amplitude and lifetime ($A \times \tau$). These lifetimes are comparable with the lifetime of the band-edge emission from CdSe QDs[29], indicating that the new short-wavelength peak that appeared after coating with gallium sulfide may originate from the band-edge transition as well.
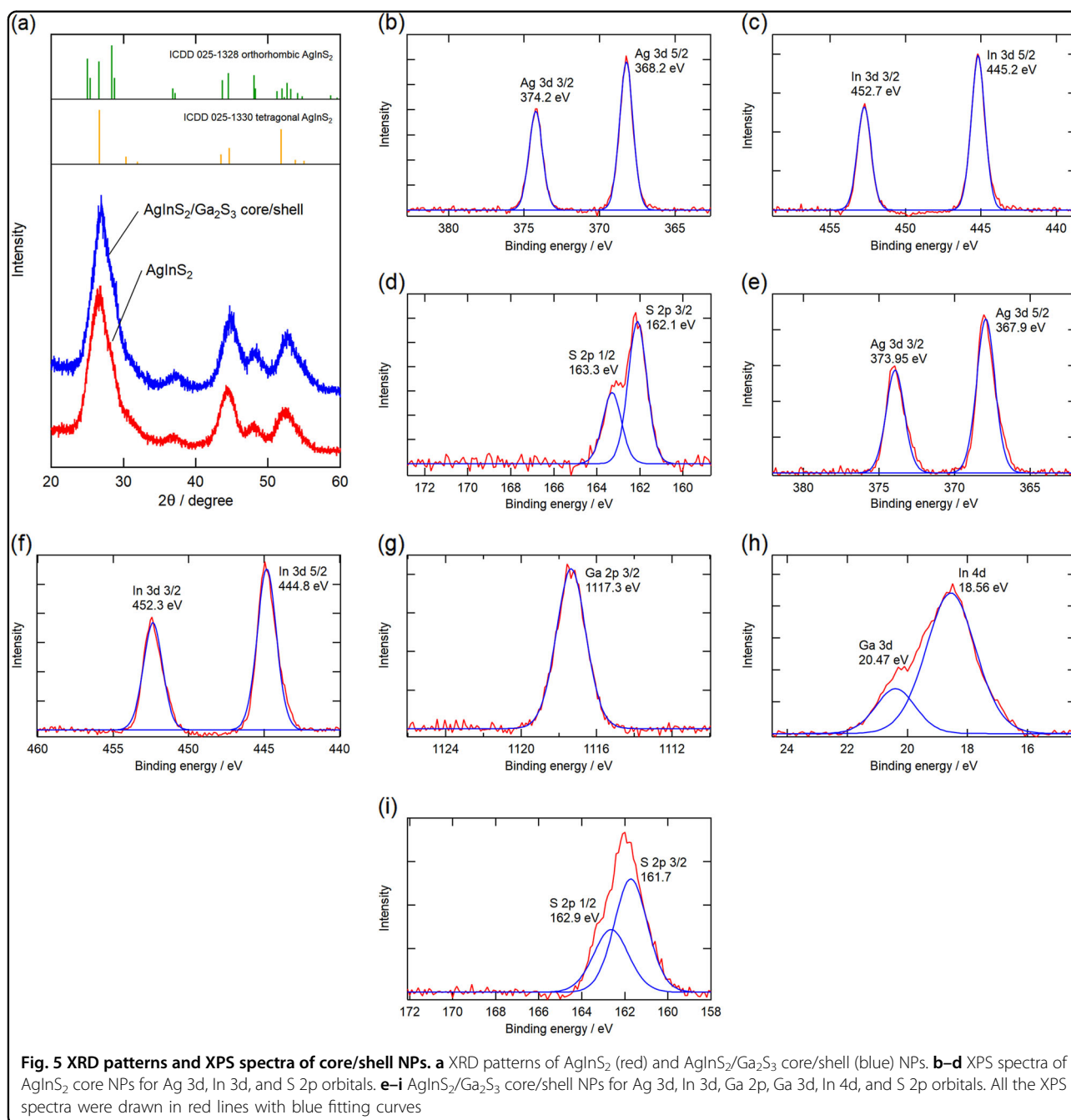
Fig. 4 TEM images and the corresponding size histograms of AgInS$_2$ and AgInS$_2$/Ga$_2$S$_3$ core/shell NPs. a TEM image and **b** size histogram for AgInS$_2$ NPs. **c** TEM image and **d** size histogram for AgInS$_2$/Ga$_2$S$_3$ core/shell NPs. **e** HRTEM and **f** HAADF-STEM images of AgInS$_2$/Ga$_2$S$_3$ core/shell NPs. Upon evaluating particle size, each particle was fit elliptically using Image-J software and evaluated as the square root of the product of major and minor axes. Size histograms, average diameter (d_{av}), and standard deviation (σ) were calculated from a few sets of TEM images including >100 nanoparticles in total

Plots of $(\alpha h\nu)^2$ as a function of $h\nu$, generally known as Tauc plots, support this interpretation (Figure S3, supplementary information). Flat regions in these plots, which appeared both for AgInS$_2$ core NPs (Fig. S3a) and for those coated with ZnS (Fig. S3b), InS$_x$ (Fig. S3c), and GaS$_x$ (Fig. S3d) shells, are spectroscopic features of direct allowed transitions and indicate their presence in these samples. The estimated bandgap was very similar between these four samples, indicating that alloying was limited under the experimental conditions used for ZnS coating. However, differences between these bandgap values and the PL peak energies, i.e., Stokes shifts, were significantly larger for the AgInS$_2$ core NPs (0.59 eV) and for those coated with ZnS (0.37 eV) and much smaller for those coated with InS$_x$ (0.05 eV) and GaS$_x$ (0.06 eV), indicating a band-edge or near band-edge emission for the latter two samples.

Structural characterization of core/shell nanoparticles

The synthesized core-only and core/shell NPs were characterized by TEM. Figure 4a, c shows TEM images of AgInS$_2$ NPs before and after the formation of gallium sulfide shells, respectively, as well as size histograms of the two types of NPs (Fig. 4b, d). The AgInS$_2$ NPs show
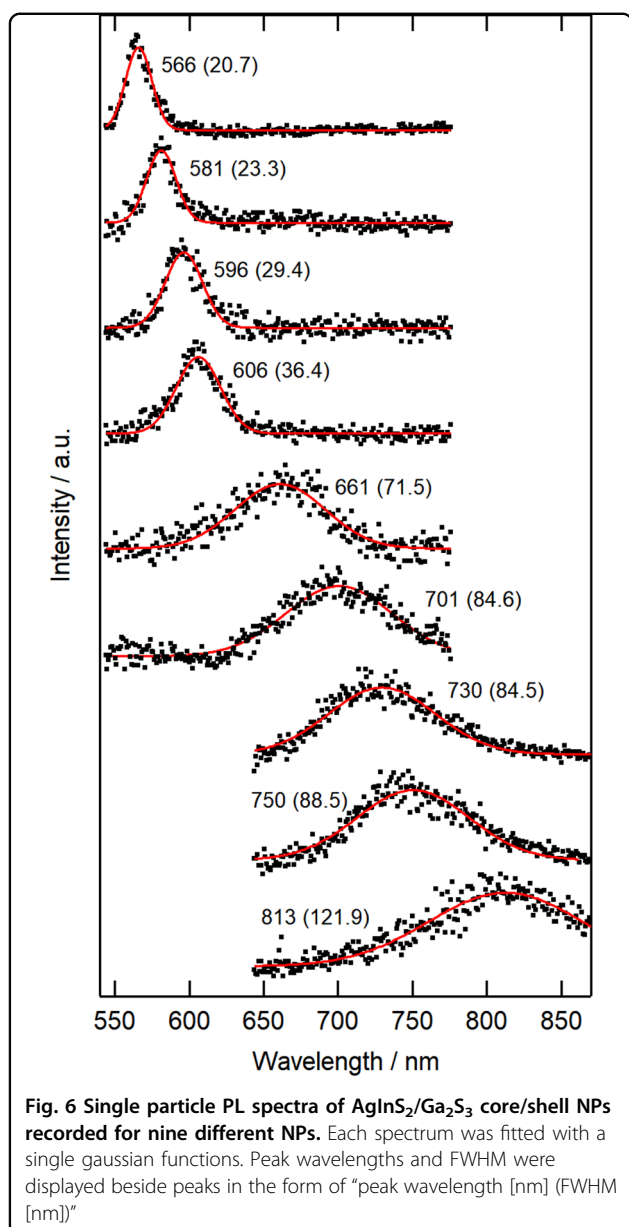
irregular, angular shapes that transition to rounded ones after the formation of the shell with a slight increase in the average particle diameter (0.4 nm) corresponding to the formation of 0.2 nm thick shell. However, the actual effect of overcoating on the average NP diameter is difficult to quantify at this stage due to the polydispersity of the original uncoated AgInS$_2$ NPs. HRTEM (Fig. 4e) and HAADF-STEM (Fig. 4f) images indicate the presence of an amorphous layer surrounding the crystalline AgInS$_2$ NPs, suggesting that the GaS$_x$ shell is amorphous. Elemental analyses for the ensemble showed an increase in gallium and sulfur after shell formation. Compared with the composition of the cores, that of the amorphous GaS$_x$ was closer to that of Ga$_2$S$_3$ rather than to that of another possible candidate, GaS (Table S1 and Figure S4, supplementary information). The amorphous nature of the shell was also supported by X-ray diffraction (XRD) analysis; the XRD patterns showed no changes in the NP crystal structure before and after the formation of the Ga$_2$S$_3$ shells (Fig. 5a). In the X-ray photoelectron spectroscopy (XPS) spectra, the positions of the peaks for silver, indium, and sulfur coincided with those of a metal sulfide, and they remained nearly unchanged during the formation of Ga$_2$S$_3$ shells, indicating that the NP cores were chemically

Fig. 5 XRD patterns and XPS spectra of core/shell NPs. a XRD patterns of AgInS$_2$ (red) and AgInS$_2$/Ga$_2$S$_3$ core/shell (blue) NPs. **b–d** XPS spectra of AgInS$_2$ core NPs for Ag 3d, In 3d, and S 2p orbitals. **e–i** AgInS$_2$/Ga$_2$S$_3$ core/shell NPs for Ag 3d, In 3d, Ga 2p, Ga 3d, In 4d, and S 2p orbitals. All the XPS spectra were drawn in red lines with blue fitting curves

unaffected by the formation of the shells (Fig. 5b, c, e, f). Although we could not obtain reference data directly for gallium sulfide, the measured peaks for gallium (Fig. 5g, h) were singular, and their position was different from that of the two possible byproducts, metal gallium and gallium oxide[30,31]. In terms of chalcogens, no additional peaks were detected for the core/shell NPs, indicating that the sulfur in the shell occurred in the form of a metal sulfide (Fig. 5i).

The concept of an amorphous shell is unusual compared with that of commonly used II–VI shells, such as

ZnS and CdS, coated onto II–VI or III–V semiconductor NPs. Generally, II–VI shells have been preferred because of their good crystallinity and expected lattice matching at the interface between the core and shell materials used. Indium and gallium sulfides possess crystal structures that are different from those of both chalcopyrite and wurtzite AgInS$_2$ and are known to contain many crystalline defects[32–34]. Therefore, these III–VI semiconductors have never been used as shell materials. However, we consider that the amorphous nature of the shell may sometimes be advantageous in

Fig. 6 Single particle PL spectra of AgInS$_2$/Ga$_2$S$_3$ core/shell NPs recorded for nine different NPs. Each spectrum was fitted with a single gaussian functions. Peak wavelengths and FWHM were displayed beside peaks in the form of "peak wavelength [nm] (FWHM [nm])"

stabilizing the complex surface elements on I–III–VI semiconductors, as this amorphous nature allows for small, continuous displacement of elements into energetically stable conformations. Similar effects have been observed for solar cells based on copper indium gallium sulfide (CIGS); in particular, the introduction of an In$_2$S$_3$ buffer layer between CIGS and n-type ZnO layers improved cell performance[35,36]. These buffer layers deposited by chemical vapor deposition (CVD) or atomic layer deposition (ALD) were reportedly amorphous in nature, although a definite correlation between the amorphous nature and improved photovoltaic performance has not been proven.

Single-particle analysis

We next used single-particle spectroscopy to gain insight into the extent of inhomogeneity in the band-edge emission. This method has been previously used to successfully uncover the multiple-defect nature of individual ZnS–AgInS$_2$ solid solution NPs and to demonstrate suppression of blinking by two-color excitation[37]. In the context of the current study, the spectra of single core/shell NPs can directly answer the important question regarding whether the residual defect emission originates from the same NPs as the bend-edge emission or whether the two types of emission derive from physically distinct particles. Figure 6 shows nine examples of PL spectra from individual NPs immobilized on a quartz substrate. The single-particle nature of the emission was confirmed by measuring the concentration dependence of the sample and by observing the PL intermittency (blinking) phenomenon (Figure S1 in the supplementary information) from individual NPs. The examples in Fig. 6 were chosen from a set of more than 250 measured NPs, each analyzed for the first 10 s of its emission. As shown in Fig. 6, the top four NPs produced only band-edge type spectra, while the bottom five NPs produced only defect-type spectra. Statistically, 50.4% of the analyzed NPs showed band-edge emission, 36.8% showed defect emission and the remaining 12.8% NPs showed both types of emission simultaneously. The same sets of spectra as a function of photon energy are shown in Figure S5 in the supplementary information together with the spectrum of an NP ensemble used for the single-particle measurements. As shown in Fig. 6, the PL FWHMs from the individual NPs were smaller than the FWHM of the ensemble spectra. This observation indicates that the ensemble PL spectra include a distribution of peak wavelengths of individual particles and are thus inhomogeneously broadened, likely due to the size distribution of the core NPs. The PL peak energy and FWHM obtained from the observation of 250 individual NPs were analyzed and plotted as histograms, as shown in Figure S6 of the supplementary information. For the band-edge emission, the mean FWHM obtained from the histogram was as small as 80.0 meV (24.0 nm). Importantly, this value is close to the PL FWHM for single CdSe/CdS/ZnS core/shell/shell QDs embedded in polymer matrices (55–65 meV) recorded at room temperature[38]. Thus, the AgInS$_2$/Ga$_2$S$_3$ core/shell NPs have considerable potential to serve as Cd-free alternatives in terms of emission properties.

Improvement of quantum yield

The low QY (12.4% for band-edge) and the remaining defect emission are major issues that must be improved for potential practical applications. Both are considered to
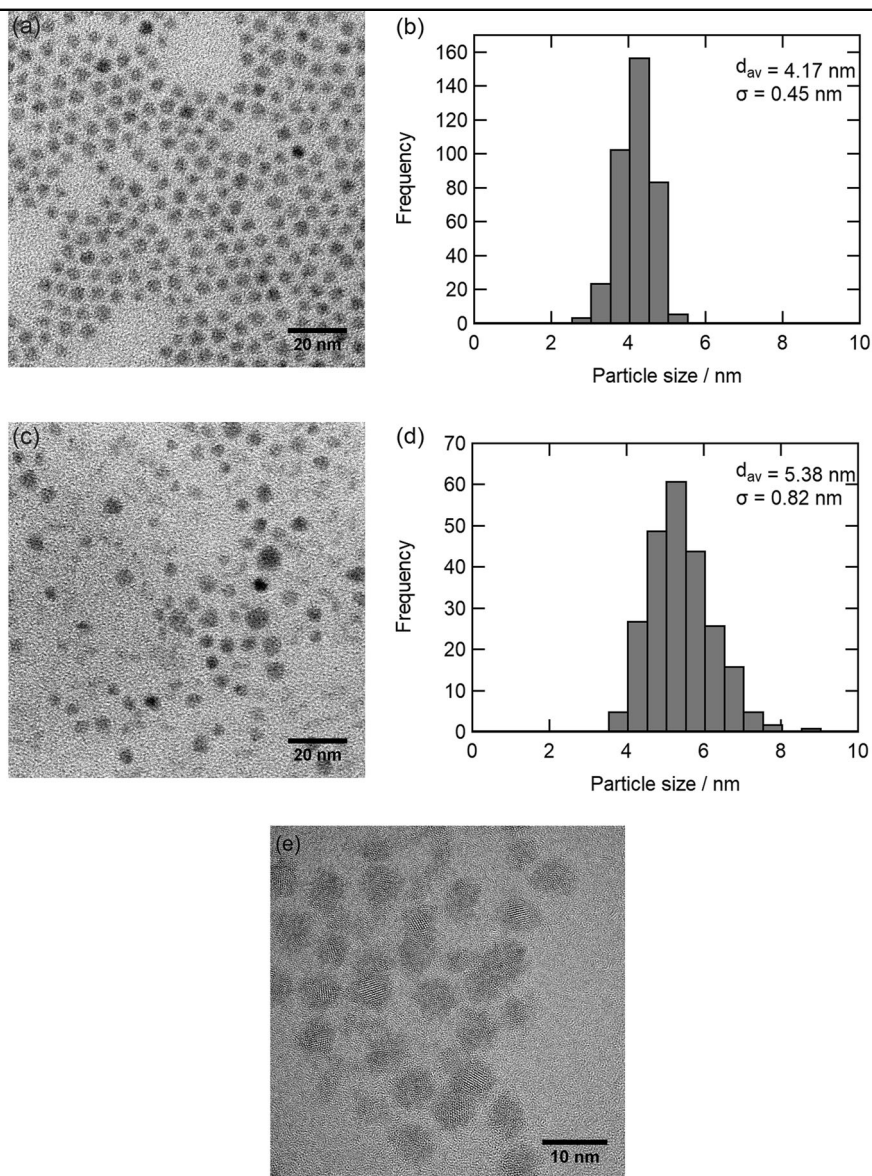
Fig. 7 TEM images and size histograms of NPs prepared using the modified procedure. a TEM image and **b** size histogram of AgInS$_2$ core NPs. **c** TEM image and **d** size histogram of AgInS$_2$/GaS$_x$ core/shell NPs. **e** HRTEM image of AgInS$_2$/GaS$_x$ core/shell NPs. Particle size was evaluated by fitting each particle elliptically and calculated as the square root of the product of two axes. Size histograms, average diameter (d_{av}), and standard deviation (σ) were calculated from a few sets of TEM images including >200 nanoparticles in total

originate from the insufficient removal of defect levels in both the core and the shell. The aforementioned 'mix everything and heating up method' used to synthesize AgInS$_2$ core NPs generates particles with large size polydispersity, as shown in the TEM image and corresponding histogram presented in Fig. 4a, b. The polydispersity originates from several types of reactions occurring simultaneously during heating to 200 °C. When the as-synthesized core NPs were size separated before the formation of gallium sulfide shells, the smaller core fractions tended to yield more intense band-edge emission, suggesting that smaller NPs have fewer defect levels

and/or are more favorably shelled. Therefore, we made modifications to the core synthesis conditions to selectively obtain smaller core NPs.

According to previous reports, AgInS$_2$ NPs are most commonly generated through Ag$_2$S as an intermediate product because Ag(I) species react more favorably with sulfur sources than with In(III) complexes. The two main roles of the intermediate Ag$_2$S are to act as seed particles on which cation exchange of Ag$^+$ and In^{3+} occurs[39] and to serve as resource hosts that operate as catalysts for the reaction of indium and sulfur sources[40]. Theoretically, the former reaction leads to an
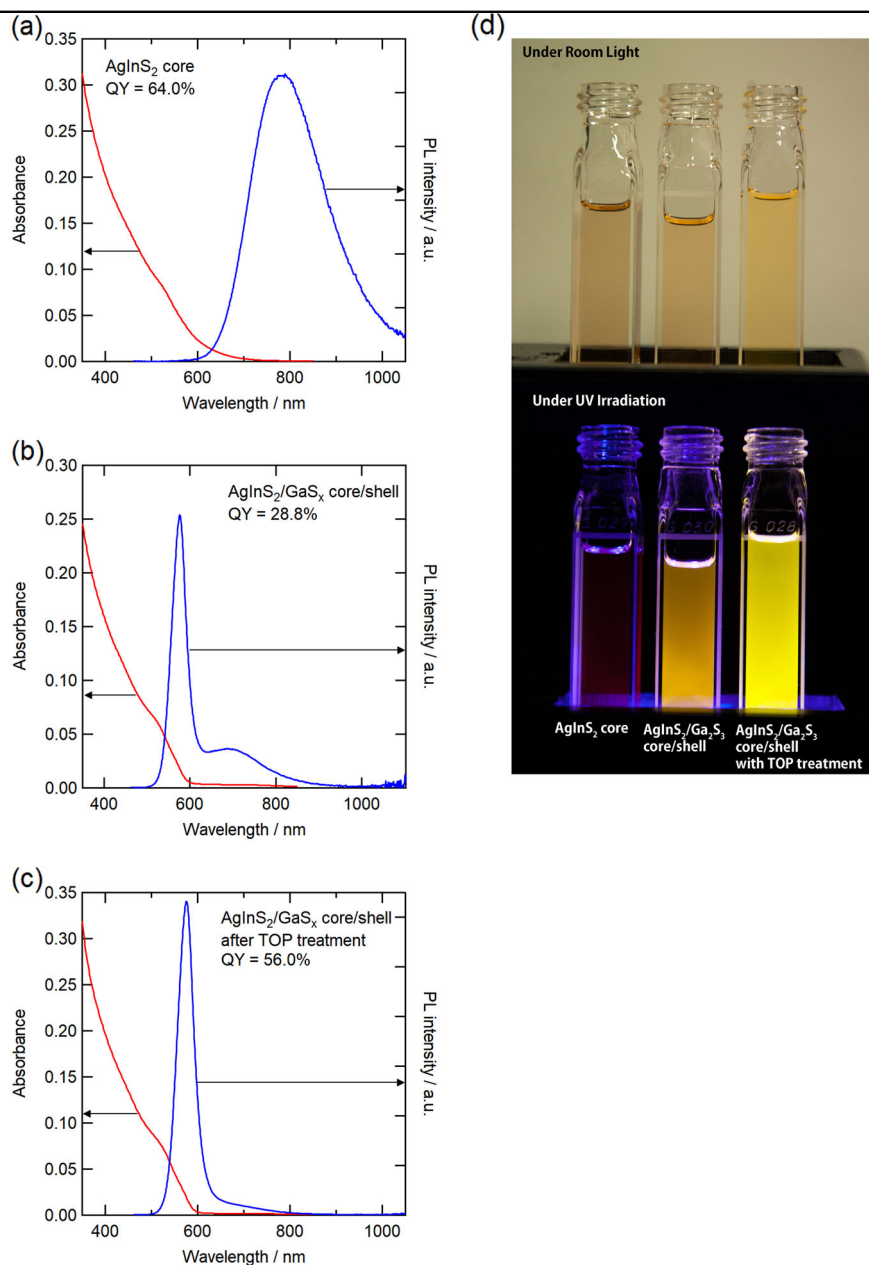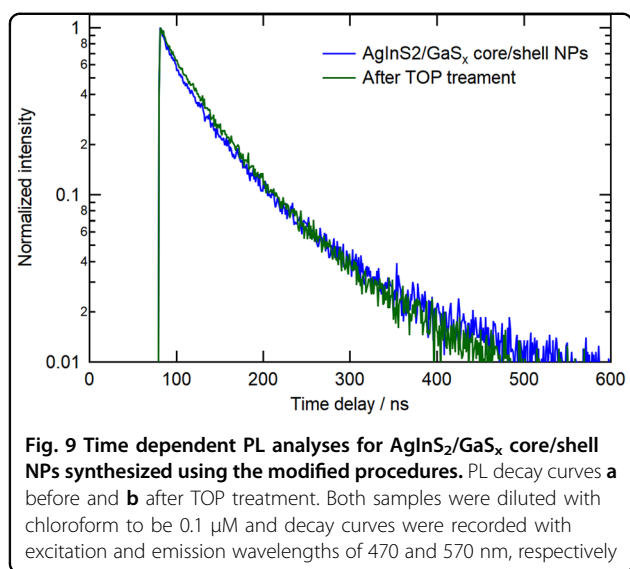
Fig. 8 Optical properties of quantum dots synthesized using the modified procedures. UV-vis and PL spectra for **a** $AgInS_2$ core NPs, **b** $AgInS_2$/GaS_x core/shell NPs, and **c** $AgInS_2$/GaS_x core/shell NPs with TOP treatment. **d** Photographs of the three samples under room light (top) and UV irradiation (bottom). Samples were diluted with chloroform to be ca. 0.05 µM and PL spectra were recorded with the excitation wavelength of 450 nm

approximately 15% decrease in particle volume, which has actually been observed[39]. The latter reaction would result in a three-fold increase in particle volume, which is undesirable in the present case. In our reaction system using thiourea as a sulfur source, the color of the solution began to change at 120 °C from yellow to orange and to dark brown, indicating the formation of Ag_2S NPs. The target $AgInS_2$ NPs were then formed at higher temperatures (>130 °C) either through cation

exchange with In(III) species (at 130 °C−150 °C) or via reaction with indium sulfide source materials generally recognized as clusters before nucleation (above 150 °C). Therefore, in this study, the reaction temperature was kept low at 135 °C for 10 min to allow for the composition of the entire NP ensemble to change to $AgInS_2$. This modified procedure successfully generated $AgInS_2$ core NPs with a smaller particle diameter and a narrower size distribution than those of particles generated

Fig. 9 Time dependent PL analyses for AgInS$_2$/GaS$_x$ core/shell NPs synthesized using the modified procedures. PL decay curves **a** before and **b** after TOP treatment. Both samples were diluted with chloroform to be 0.1 μM and decay curves were recorded with excitation and emission wavelengths of 470 and 570 nm, respectively

previously (Fig. 7a, b). The PL QY of the core NPs was 64% (Fig. 8a), which is a record high value for AgInS$_2$ core-only NPs, even though the spectral shape is that of broad defect emission.

For the shell formation reaction, the sulfur source was changed from elemental sulfur to 1,3-dimethylthiourea, which reacts with Ga(acac)$_3$ at higher temperatures (>230 °C) to generate gallium sulfide. Although elemental sulfur is a common sulfur source for many chalcogenide nanoparticles, we observed that it has a strong quenching effect on the PL of AgInS$_2$ core NPs. Undesired contact with elemental sulfur in the early stage of the shell formation reaction could thus be avoided by the use of the sulfur compound. In addition, the change in atomic ratio between gallium and sulfur (from Ga:S = 1:1.5 to 1:1) led to gallium-rich conditions. The temperature gradient was also modified in accordance with the decomposition of 1,3-dimethylthiourea to avoid the nucleation of gallium sulfide as much as possible. These modifications to the synthesis protocol improved the PL QY of the AgInS$_2$/GaS$_x$ core/shell NPs to 15–20% for the band-edge emission and to 25−30% for the entire spectral region (Fig. 8b). For the band-edge emission, this increase represents an improvement by a factor of 1.5 over the PL QY obtained using the original synthesis conditions. The thickness of the shell, calculated from the average diameter change before and after shell formation, was increased from 0.2 nm for the previous method to 0.6 nm (Fig. 7b, d), although the shell was still thinner than the expected value (1 nm) calculated based on the amount of materials. An HRTEM image clearly shows the existence of 0.5–1.0 nm amorphous shells around crystalline cores measuring 3–5 nm in diameter, depending on location (Fig. 7e). The difference between the expected bandgap and PL peak energy became even smaller (0.02 eV),

indicating better passivation (Figure S3e, supplementary information). Further improvement of the PL QY was achieved by post-treatment of the AgInS$_2$/GaS$_x$ core/shell NPs with TOP. The post-treatment was carried out after removing the NPs from the solution used for shell formation. The intensity of the band-edge emission nearly doubled within a few hours in the presence of TOP, with a slight decrease in the remaining defect emission, keeping the UV–vis absorption profile nearly unchanged (Fig. 8c). As a result, nearly single-band emission with a QY as high as 56% was obtained with high reproducibility, yielding a brilliant yellow emission bright enough to observe under ambient light (Fig. 8d and Figure S7, supplementary information). The crystal structures of the AgInS$_2$ core and AgInS$_2$/GaS$_x$ core/shell NPs were similar to those prepared by the original method, but a purer tetragonal phase was observed (Figure S8, supplementary information). These findings are well consistent with a previous report by Doh et al.[39] that showed that 4 nm Ag$_2$S NPs were converted to tetragonal AgInS$_2$ NPs, while larger (8 nm) NPs were transformed into orthorhombic AgInS$_2$ NPs, upon cation exchange with In^{3+} species. According to that report, Ag$_2$S seed particles are prone to conversion to orthorhombic AgInS$_2$, which is structurally more favorable, whereas the thermodynamically more stable tetragonal phase can be generated when the particle size is small enough (<4.5 nm for seed Ag$_2$S) to invoke a rearrangement.

The remarkable improvement in PL QY by the TOP treatment was surprising, and we offer the following hypothesis. The gallium sulfide shell passivates the defect levels on the surface of the AgInS$_2$ core NPs, which leads to the generation of the band-edge emission. However, excitons could still be leaking outside of the core due to an insufficient potential barrier between the core and the thin amorphous gallium sulfide shells. The major traps for electrons were, potentially, zero-valent sulfur sites existing on the surface of the gallium sulfide shell. These traps operate as acceptors for photogenerated electrons. TOP is well known to coordinate with chalcogens; therefore, the TOP treatment has the potential to passivate the electron traps on the surface of the gallium sulfide shells, either by

Table 2 PL decay components for AgInS$_2$/GaS$_x$ core/shell NPs synthesized using the modified procedures before and after TOP treatment

Sample		A_1, τ_1	A_2, τ_2	A_3, τ_3	x^2
AgInS$_2$/GaS$_x$ core/shell	A	0.339	0.592	0.069	1.24
	τ/ns	9.5	52.3	203.4	
After TOP treatment	A	0.204	0.704	0.092	1.06
	τ/ns	8.8	50.5	157.5	

filling electrons in the LUMO level of the surface sulfur sites or by removing the sulfur sites via conversion to a more stable tri-*n*-octylphosphine sulfide. Elemental analyses of the core/shell NPs synthesized with the modified procedure showed a decrease in the ratio of sulfur in the shell (to Ga:S = 1:0.84) from that observed for the shells synthesized using elemental sulfur with a 1.5 equivalent of Ga(acac)$_3$ (Table S2 and Figure S9, supplementary information). The abovementioned observations suggest that the amount and valency of sulfur may be key factors controlling the PL QY of core/shell NPs.

Unexpectedly, however, the PL decay curves obtained before and after the TOP treatment did not show such drastic changes (Fig. 9). The PL lifetimes, which nearly doubled those of the core/shell NPs synthesized using >6 nm cores and elemental sulfur for the shell source material (Table 1), remained unchanged after the TOP treatment (Table 2). These results suggest suppression of blinking, which itself is generally caused by NP charging. We indeed observed strong blinking with long off-times for the AgInS$_2$/GaS$_x$ core/shell NPs synthesized by the first method (Figure S1, supplementary information), similar to the blinking behavior of uncoated core NPs[37]. However, Figure S10 shows the time traces of PL intensity of individual core/shell NPs synthesized with the modified method before and after TOP treatment. The core/shell NPs without TOP treatment (Figure S10, bottom, red-traces) showed short 'on' durations with an on/off frequency often higher than the recording frame rate (20 Hz). This behavior was substantially altered by the addition of TOP, which resulted in longer and more stable 'on' states (Figure S10, top, blue traces). Therefore, the doubling of the PL QY by TOP treatment is mostly attributed to the increase in 'on' duration and was likely caused by the effective blocking of charges from escaping from the core. In addition, it is worth mentioning that the TOP-treated core/shell NPs exhibited a PL QY of 56.0%, which is comparable to that of the core NPs (64%), suggesting that we were successful in altering the pathway of photogenerated carriers without causing a significant efficiency loss. Studies aimed at further increasing the PL QY and identifying the quantitative aspects of the corresponding excitonic characteristics are underway.

Conclusions

In summary, we have demonstrated band-edge emission from AgInS$_2$ NPs by coating them with III–VI semiconductors, GaS$_x$ shells, with a composition ranging from $x = 0.8$ to $x = 1.5$. The new band-edge PL band has a FWHM as small as 30 nm in an ensemble and 20 nm at the single-particle level. The core/shell structure was successfully observed by HRTEM and STEM, which showed that, unlike conventional crystalline II–VI semiconductors shells, the GaS$_x$ shell was amorphous. The

successful demonstration of surface trap removal by the amorphous layer may indicate a new direction in the design of core/shell nanostructures. Similarly to the role of organic ligands that bind to specific elements to remove intra-bandgap defect levels, 'soft' non-crystalline inorganic shells might prove advantageous in stabilizing ternary, quaternary semiconductor NPs that have complex surface structures. In terms of PL QY, the AgInS$_2$ NP cores obtained using the 'mix everything and heating up method' demonstrated a value representing 12.4% of the band-edge emission after coating with gallium sulfide. This value was further improved dramatically by several modifications to the synthetic conditions, for both core and shell syntheses, and by post-treatment of the core/shell NPs with TOP. Nearly single-band-edge emission with a PL QY as high as 56% was obtained by the modified synthetic procedures. These findings indicate that the core/shell AgInS$_2$ NPs are nearly comparable to cadmium chalcogenide QDs. The elucidation of the band-edge emission mechanism is underway, with the goal of further improving the PL QY and monochromaticity.

Author details

[1]Frontier Research Base for Global Young Researchers, Graduate School of Engineering, Osaka University, 2-1 Yamada-oka, Suita, Osaka 565-0871, Japan. [2]Department of Applied Chemistry, Graduate School of Engineering, Osaka University, 2-1 Yamada-oka, Suita, Osaka 565-0871, Japan. [3]Department of Materials Science and Engineering, Tokyo Institute of Technology, 2-12-1 Ookayama, Meguro, Tokyo 152-8552, Japan. [4]Department of Quantum Engineering, Graduate School of Engineering, Nagoya University, Chikusa-ku, Nagoya 464-8603, Japan. [5]Department of Crystalline Materials Science, Graduate School of Engineering, Nagoya University, Chikusa-ku, Nagoya 464-8603, Japan

Conflict of interest

Two of the research groups represented by S.K. (Osaka University) and T.T. (Nagoya University) have been funded by the Nichia Corporation. The other authors declare that they have no conflict of interest.

Publisher's note

Springer Nature remains neutral with regard to jurisdictional claims in published maps and institutional affiliations.

References

1. Murray, C. B., Norris, D. J. & Bawendi, M. G. Synthesis and characterization of nearly monodisperse CdE (E = S, Se, Te) semiconductor nanocrystallites. *J. Am. Chem. Soc.* **115**, 8706–8715 (1993).

2. Qu, L. & Peng, X. Control of photoluminescence properties of CdSe nanocrystals in growth. *J. Am. Chem. Soc.* **124**, 2049–2055 (2002).

3. Chen, O. et al. Compact high-quality CdSe-CdS core-shell nanocrystals with narrow emission linewidths and suppressed blinking. *Nat. Mater.* **12**, 445–451 (2013).

4. Frecker, T., Bailey, D., Arzeta-Ferrer, X., McBride, J. & Rosenthal, S. J. Quantum dots and their application in lighting, displays, and biology. *ECS J. Solid State Sci. Technol.* **5**, R3019–R3031 (2016).

5. Battaglia, D. & Peng, X. G. Formation of high quality InP and InAs nanocrystals in a noncoordinating solvent. *Nano Lett.* **2**, 1027–1030 (2002).

6. Kim, S. et al. Highly luminescent InP/GaP/ZnS nanocrystals and their application to white light-emitting diodes. *J. Am. Chem. Soc.* **134**, 3804–3809 (2012).

7. Xu, S., Kumar, S. & Nann, T. Rapid synthesis of high-quality InP nanocrystals. *J. Am. Chem. Soc.* **128**, 1054–1055 (2006).

8. Torimoto, T. et al. Facile synthesis of ZnS–$AgInS_2$ solid solution nanoparticles for a color-adjustable luminophore. *J. Am. Chem. Soc.* **129**, 12388–12389 (2007).

9. Allen, P. M. & Bawendi, M. G. Ternary I-III-VI quantum dots luminescent in the red to near-infrared. *J. Am. Chem. Soc.* **130**, 9240–9241 (2008).

10. Omata, T., Nose, K. & Otsuka-Yao-Matsuo, S. Size dependent optical band gap of ternary I-III-VI_2 semiconductor nanocrystals. *J. Appl. Phys.* **105**, 073106–073105 (2009).

11. Torimoto, T., Kameyama, T. & Kuwabata, S. Photofunctional materials fabricated with chalcopyrite-type semiconductor nanoparticles composed of $AgInS_2$ and its solid solutions. *J. Phys. Chem. Lett.* **5**, 336–347 (2014).

12. Hamanaka, Y., Ogawa, T., Tsuzuki, M. & Kuzuya, T. Photoluminescence properties and its origin of $AgInS_2$ quantum dots with Chalcopyrite structure. *J. Phys. Chem. C.* **115**, 1786–1792 (2011).

13. Rao, M. J., Shibata, T., Chattopadhyay, S. & Nag, A. Origin of photoluminescence and XAFS study of $(ZnS)_{1-x}(AgInS_2)_x$ nanocrystals. *J. Phys. Chem. Lett.* **5**, 167–173 (2014).

14. Zaiats, G., Kinge, S. & Kamat, P. V. Origin of dual photoluminescence states in ZnS–$CuInS_2$ alloy nanostructures. *J. Phys. Chem. C* **120**, 10641–10646 (2016).

15. Sandroni, M., Wegner, K. D., Aldakov, D. & Reiss, P. Prospects of Chalcopyrite-type nanocrystals for energy applications. *ACS Energy Lett.* **2**, 1076–1088 (2017).

16. Jara, D. H., Stamplecoskie, K. G. & Kamat, P. V. Two distinct transitions in Cu_xInS_2 quantum dots. Bandgap versus sub-bandgap excitations in copper-deficient structures. *J. Phys. Chem. Lett.* **7**, 1452–1459 (2016).

17. Kameyama, T. et al. Crystal phase-controlled synthesis of rod-shaped $AgInTe_2$ nanocrystals for in vivo imaging in the near-infrared wavelength region. *Nanoscale* **8**, 5435–5440 (2016).

18. Reiss, P., Protiére, M. & Li, L. Core/shell semiconductor nanocrystals. *Small* **5**, 154–168 (2009).

19. Xie, R., Rutherford, M. & Peng, X. Formation of high-quality I–III–VI semiconductor nanocrystals by tuning relative reactivity of cationic precursors. *J. Am. Chem. Soc.* **131**, 5691–5697 (2009).

20. Dabbousi, B. O. et al. (CdSe)ZnS core–shell quantum dots: synthesis and characterization of a size series of highly luminescent nanocrystallites. *J. Phys. Chem. B* **101**, 9463–9475 (1997).

21. Akkerman, Q. A. et al. From binary Cu_2S to ternary Cu–In–S and quaternary Cu–In–Zn–S nanocrystals with tunable composition via partial cation exchange. *ACS Nano* **9**, 521–531 (2015).

22. De Trizio, L. et al. Strongly fluorescent quaternary Cu–In–Zn–S nanocrystals prepared from $Cu_{1-x}InS_2$ nanocrystals by partial cation exchange. *Chem. Mater.* **24**, 2400–2406 (2012).

23. Song, J. et al. Bandgap and structure engineering via cation exchange: from binary Ag_2S to ternary $AgInS_2$, quaternary AgZnInS alloy and AgZnInS/ZnS core/shell fluorescent nanocrystals for bioimaging. *ACS Appl. Mater. Inter.* **8**, 24826–24836 (2016).

24. Sachanyuk, V. P., Gorgut, G. P., Atuchin, V. V., Olekseyuk, I. D. & Parasyuk, O. V. The Ag_2S–In_2S_3–$Si(Ge)S_2$ systems and crystal structure of quaternary sulfides $Ag_2In_2Si(Ge)S_6$. *J. Alloy. Compd.* **452**, 348–358 (2008).

25. Tsuji, I., Kato, H., Kobayashi, H. & Kudo, A. Photocatalytic H_2 evolution reaction from aqueous solutions over band structure-controlled $(AgIn)_xZn_{2(1-x)}S_2$ solid solution photocatalysts with visible-light response and their surface nanostructures. *J. Am. Chem. Soc.* **126**, 13406–13413 (2004).

26. Dana, J., Debnath, T. & Ghosh, H. N. Involvement of sub-bandgap states in subpicosecond exciton and biexciton dynamics of ternary $AgInS_2$ nanocrystals. *J. Phys. Chem. Lett.* **7**, 3206–3214 (2016).

27. Smith, A. M. & Nie, S. Semiconductor nanocrystals: structure, properties, and band gap engineering. *Acc. Chem. Res.* **43**, 190–200 (2010).

28. Ivashchenko, I. A., Danyliuk, I. V., Olekseyuk, I. D., Pankevych, V. Z. & Halyan, V. V. Phase equilibria in the quasiternary system Ag_2S–Ga_2S_3–In_2S_3 and optical properties of $(Ga_{55}In_{45})_2S_{300}$, $(Ga_{54.59}In_{44.66}Er_{0.75})_2S_{300}$ single crystals. *J. Solid State Chem.* **227**, 255–264 (2015).

29. Uematsu, T., Shimomura, E., Torimoto, T. & Kuwabata, S. Evaluation of surface ligands on semiconductor nanoparticle surfaces using electron transfer to redox species. *J. Phys. Chem. C* **120**, 16012–16023 (2016).

30. Hou, X. Y. et al. Electrochemical sulfur passivation of GaAs. *Appl. Phys. Lett.* **60**, 2252–2254 (1992).

31. Papis, E. et al. Sulphur passivation of GaSb, InGaAsSb and AlGaAsSb surfaces. *Phys. Stat. Sol. (C)* **4**, 1448–1453 (2007).

32. Aydinli, A., Gasanly, N. M. & Gökşen, K. Donor–acceptor pair recombination in gallium sulfide. *J. Appl. Phys.* **88**, 7144–7149 (2000).

33. Yu, S. et al. Hydrothermal preparation and characterization of nanocrystalline powder of β-indium sulfide. *Mater. Res. Bull.* **33**, 717–721 (1998).

34. Rehwald, W. & Harbeke, G. On the conduction mechanism in single crystal β-indium sulfide In_2S_3. *J. Phys. Chem. Solids* **26**, 1309–1324 (1965).

35. Yousfi, E. B., Weinberger, B., Donsanti, F., Cowache, P. & Lincot, D. Atomic layer deposition of zinc oxide and indium sulfide layers for $Cu(In,Ga)Se_2$ thin-film solar cells. *Thin Solid Films* **387**, 29–32 (2001).

36. Yousfi, E. B. et al. Cadmium-free buffer layers deposited by atomic later epitaxy for copper indium diselenide solar cells. *Thin Solid Films* **361–362**, 183–186 (2000).

37. Sharma, D. K. et al. Single-particle spectroscopy of I-III-VI semiconductor nanocrystals: spectral diffusion and suppression of blinking by two-color excitation. *Nanoscale* **8**, 13687–13694 (2016).

38. Gómez, D. E., van Embden, J. & Mulvaney, P. Spectral diffusion of single semiconductor nanocrystals: the influence of the dielectric environment. *Appl. Phys. Lett.* **88**, 154106 (2006).

39. Doh, H., Hwang, S. & Kim, S. Size-tunable synthesis of nearly monodisperse Ag_2S nanoparticles and size-dependent fate of the crystal structures upon cation exchange to $AgInS_2$ nanoparticles. *Chem. Mater.* **28**, 8123–8127 (2016).

40. Zhu, G. & Xu, Z. Controllable growth of semiconductor heterostructures mediated by bifunctional Ag_2S nanocrystals as catalyst or source-host. *J. Am. Chem. Soc.* **133**, 148–157 (2011).